Am J Nucl Med Mol Imaging 2013;3(2):142-153
www.ajnmmi.us /ISSN:2160-8407/ajnmmi1211003

Original Article

^{18}F-misonidazole PET imaging of hypoxia in micrometastases and macroscopic xenografts of human non-small cell lung cancer: a correlation with autoradiography and histological findings

Tao Huang[1,2,3], A Cahid Civelek[4], Huaiyu Zheng[3], Chin K Ng[3], Xiaoxian Duan[3], Junling Li[3], Gregory C Postel[3], Baozhong Shen[1,2], Xiao-Feng Li[3]

[1]Department of Radiology, the 4th Hospital of Harbin Medical University, Harbin, Heilongjiang, China; [2]Key Laboratory of Molecular Imaging, College of Heilongjiang Province, Harbin, Heilongjiang, China; [3]Department of Diagnostic Radiology, [4]Division of Nuclear Medicine, University of Louisville School of Medicine, Louisville, Kentucky USA

Received November 19, 2012; Accepted January 28, 2013; Epub March 8, 2013; Published March 18, 2013

Abstract: The objective of this study was to determine whether ^{18}F-misonidazole could detect hypoxia in macroscopic and microscopic tumors in mice. In nude mice, subcutaneous xenografts and peritoneal metastases were generated utilizing human non-small cell lung cancer A549 and HTB177 cells. Animals were co-injected with ^{18}F-misonidazole, pimonidazole and bromodeoxyuridine, and tumor perfusion was assessed by Hoechst 33342 injection. The intratumoral distribution of ^{18}F-misonidazole was determined by micro-PET scan and autoradiography. Pimonidazole, bromodeoxyuridine and Hoechst 33342 were detected by immunohistochemistry on the autoradiography sections. Submillimeter micrometastases found to be severely hypoxic. In both peritoneal metastases and subcutaneous xenografts models, PET images displayed significant ^{18}F-misonidazole uptake, and its distribution was non-uniform in these macroscopic subcutaneous tumors. In frozen sections, digital autoradiography and immunohistochemistry revealed similar distributions of ^{18}F-misonidazole, pimonidazole and glucose transporter-1, in both microscopic and macroscopic tumors. Bromodeoxyuridine stained-positive proliferative regions were well perfused, as judged by Hoechst 33342, and displayed low ^{18}F-misonidazole accumulation. ^{18}F-misonidazole uptake was low in tumor stroma and necrotic zones as well. Microscopic non-small cell lung cancer metastases are severely hypoxic. ^{18}F-misonidazole PET is capable to image hypoxia noninvasively not only in macroscopic tumors but also in micrometastases growing in mice. Accordingly, ^{18}F-misonidazole may be a promising agent to detect the burden of micrometastatic diseases.

Keywords: Micrometastasis, hypoxia, ^{18}F-misonidazole, PET, autoradiography

Introduction

Lung cancer is responsible for more deaths than any other cancer [1], and approximately 85% human lung cancers are non-small cell lung cancer. Most lung cancer-related deaths are due to the development of metastatic disease rather than the progression of the primary tumor [2]. Regions of local hypoxia are common features of many human primary solid cancers [3-6]. We have recently found that, in an animal model of colorectal cancer micrometastases, peritoneal cavity microscopic tumors of less than 1 mm diameter were extremely hypoxic [7-10]. However, the status of hypoxia in lung cancer micrometastases is largely unknown.

It has been established that hypoxic cancer cells are more resistant than aerobic cells to ionizing radiation and chemotherapy. Thus, tumor hypoxia is an important determinant of relapse-free survival and overall clinical outcome [5, 11, 12]. In studies of macroscopic tumors, hypoxia can be assessed by pO_2 probe measurements and non-invasive imaging with radiolabeled hypoxic tracers. For micrometastases however, assessing of hypoxia may required invasive methods [8], relying on detection of either an exogenous substance such as

2-nitroimidazole compounds pimonidazole, EF5 and CCI-103F, which are selectively reduced in hypoxic regions of the tumors (generally when pO_2 <10 mmHg) [13] or the expression of endogenous markers of hypoxia such as hypoxia inducible factor 1α (HIF1α), carbonic anhydrase 9 and glucose transporters 1 and 3 [8]. Microscopically spatial pattern of binding of these markers can be visualized on tumor sections by immunohistochemical methods. In an analogous approach, the spatial pattern of binding of radiolabeled hypoxia tracers in tumor sections may be visualized by autoradiography. Radiolabeled tracers including ^{18}F-misonidazole [14-16], copper (II)-diacetyl-bis(N(4)-methylthiosemicarbazone [17-19] and ^{124}I-labeled iodo-azomycin galactopyranoside [20-22] amongst others have developed for imaging tumor hypoxia.

Since the presence and the degree of tumor hypoxia effects the disease outcome in patients, from the disease management point of view the ability to noninvasively detect hypoxia in tumor or in its metastasis has a great clinical importance. While ^{18}F-misonidazole is the most frequently used PET tracer for detecting hypoxia in the clinical settings [23-26], its value for imaging hypoxia of microscopic diseases, including in micrometastases of non-small cell lung cancer has not been established. It is expected that ^{18}F-misonidazole PET detect hypoxia in macroscopic xenografts. Although it may be difficult to image hypoxia of a solitary, single micrometastases with PET, a collection of multiple such severely hypoxic deposits of micrometastases may be easily detected by PET utilizing ^{18}F-misonidazole. We tested this hypothesis in mouse models of human non-small cell lung cancer.

In this study, we used noninvasive ^{18}F-misonidazole PET and invasive correlative imaging methods to examine the hypoxia status in both microscopic and macroscopic tumors of human non-small cell lung cancer and relate this to hypoxic status as determined by pimonidazole and glucose transporter-1 immunohistochemistry.

Materials and methods

Tumor cell lines and animals

The human non-small cell lung cancer A549 and HTB177 cell lines were purchased from American Type Culture Collection (Manassas, VA). and maintained in F-12K Medium (Manassas, VA) and RPMI 1640 medium (Cellgro, Herndon, VA), respectively. All media were supplemented with 10% fetal bovine serum (Gemini, West Sacramento, CA), 1% glutamine and 1% antibiotic mixture (Cellgro). Cells were grown in humidified incubator at 37°C with 5% carbon dioxide. Exponentially growing cells were harvested with 0.25% (w/v) Trypsin-0.53 mM EDTA solution, washed and suspended in phosphate buffered saline (PBS). The number of viable cells was counted using a Vi-CELL™ cell viability analyzer (Beckman-Coulter, Miami, FL).

All experiments were performed using 6-week-old female athymic NCr-*nu/nu* mice purchased from NCI-Frederick Cancer Research Institute (Bethesda, MD). Nude mice were maintained and used according to the guidelines of University of Louisville Health Center Animal Care and Use Committee. Animals were housed five *per* cage and kept in the institutional small animal facility at a constant temperature and humidity. Food pellets and water were provided *ad libitum*.

Establishment of tumors in mice

Disseminated microscopic tumors were induced in the peritoneum by injecting tumor cell suspensions (5×10^6 cells/0.2ml) into the peritoneal cavity. Animals were used for experiments approximately 4 weeks after injection. At this time, a distribution of tumors of varying sizes was observed to be present. Subcutaneous tumors were initiated by injecting 5×10^6 tumor cells in 0.1 ml PBS subcutaneously into each of mouse flanks. Experiments were performed when tumors reached approximately 1 cm in average diameter which occurred typically 3-4 weeks after initiation.

Radiotracers

^{18}F-FDG and ^{18}F-fluoride was purchased from P.E.T. NET Pharmaceuticals Inc. facility at University of Louisville Hospital. ^{18}F- misonidazole was prepared with an automated modular-lab system (Eckert & Ziegler; Berlin, Germany) as described previously *(27).* In brief, ^{18}F-fluoride was passed through a QMA cartridge and eluted with 0.5 ml of tetrabutylammonium bicarbonate (75 mM) into the reaction vessel. Dry

acetonitrile (1 ml) was added into the reaction vessel and heated with the help of nitrogen flow until completely dry. 10 mg of the precursor 3-(2-Nitroimidazol-1-yl)-2-O-tetrahydropyranyl-1-O-toluenesulfonylpropanediol (ABX, Radeberg, Germany) in 100 μl of CH_3CN and 500 μl of t-butanol was added and reacted for 15 min at 105°C, followed by hydrolysis with 1 N HCl (1 ml) at 105°C for 10 min. After cooling down to room temperature, 1N sodium acetate (1 ml) was added and then delivered to semi-preparative C18 HPLC for purification. Radiochemical yields thin layer chromatography was approximately 70%. Radiochemical purity was greater than 99%.

Markers of hypoxia, proliferation and perfusion

The hypoxia marker, pimonidazole hydrochloride (1-[(2-hydroxy-3-piperidinyl)propyl]-2-nitroimidazole hydrochloride) (Hypoxyprobe Inc, Burlington, MA) was dissolved in physiological saline at a concentration of 20 mg/ml. The proliferation marker, bromodeoxyuridine (Roche Diagnostics, Indianapolis, IN) was first dissolved in dimethyl sulfoxide and further diluted in physiological saline to a final concentration of 20 mg/ml. The blood perfusion marker, Hoechst 33342 (Sigma-Aldrich, St. Louis, MO) was dissolved in physiological saline at a concentration of 5 mg/ml. In all cases, fresh drug solutions were prepared on the day of injection.

Micro-PET imaging

All animals were imaged in a prone position using the dedicated three-dimensional small-animal R4 micro-PET (Concorde Microsystems, Knoxville, TN) system. The R4 microPET scanner has a transaxial field of view of 10 cm and an axial field of view of 7.8 cm. The resulting list-mode data were sorted into two-dimensional histograms by Fourier rebinning, and the images reconstructed by an iterative reconstruction algorithm into a 128 × 128 × 63 (0.72 × 0.72 × 1.3 mm) matrix. No attenuation or scatter correction was applied. All animals were not fasted before experiments unless stated otherwise.

Mice were injected via the tail vein with a mixture of ^{18}F- misonidazole (~7.4 MBq), pimonidazole (2 mg) and bromodeoxyuridine (4 mg) without anesthesia; the total injection volume was 0.4 ml for each mouse. Two hours after tracer injection, animals were anesthetized by inhalation of an isoflurane (1.5%)–air mixture and maintained throughout the PET scan. In all experiments, acquisition time was fixed to10 min for each PET scan. After PET scan, Hoechst 33342 (0.5 mg, 0.1 ml) was injected via the tail veins and animals were sacrificed 1-2 min later. Both microscopic tumors and macroscopic subcutaneous xenografts were studied. We included 5 mice with A549 peritoneal metastases, 5 mice with HTB177 peritoneal diseases, and 5 mice, each bearing an A549 xenograft the right frank and a HTB177 tumor on the other side.

In one group of animals of 4, one day before ^{18}F-misonidazole PET study, ^{18}F-FDG (~7.4 MBq) was injected in overnight fasting animals and ^{18}F-FDG PET was performed 1h later to compare with ^{18}F-misonidazole PET imaging.

PET image analysis

All image sets for each animal were visually examined using a rotating (cine) three-dimensional display. The window and level settings were adjusted for best intratumoral distribution visibility. The images were assessed subjectively, and a report produced on the salient features of the activity distribution within the tumor.

Subsequently, the image data sets for each animal were aligned manually in three dimensions using the multiple image analysis utility software application. ASIPro VM microPET analysis software (Concorde Microsystems Inc) was used for analysis. Once the image sets were aligned, a region of interest was manually drawn to circumscribe the visible tumor or intratumoral component outline on a mid-coronal tumor slice, depending on the projection at which the tumor was best visualized.

Preparation of frozen tumor sections

As we described previously [7, 9, 10, 27], immediately after animal sacrifice, tumor tissues were removed for subsequent processing. Subcutaneous xenografts were frozen and embedded in embedding in optimal cutting temperature (O.C.T.) compound (Sakura Finetek, Torrance Ca). Peritoneal tumors (adhering to the intestinal serosa) were washed with cold PBS to remove any attached ascites

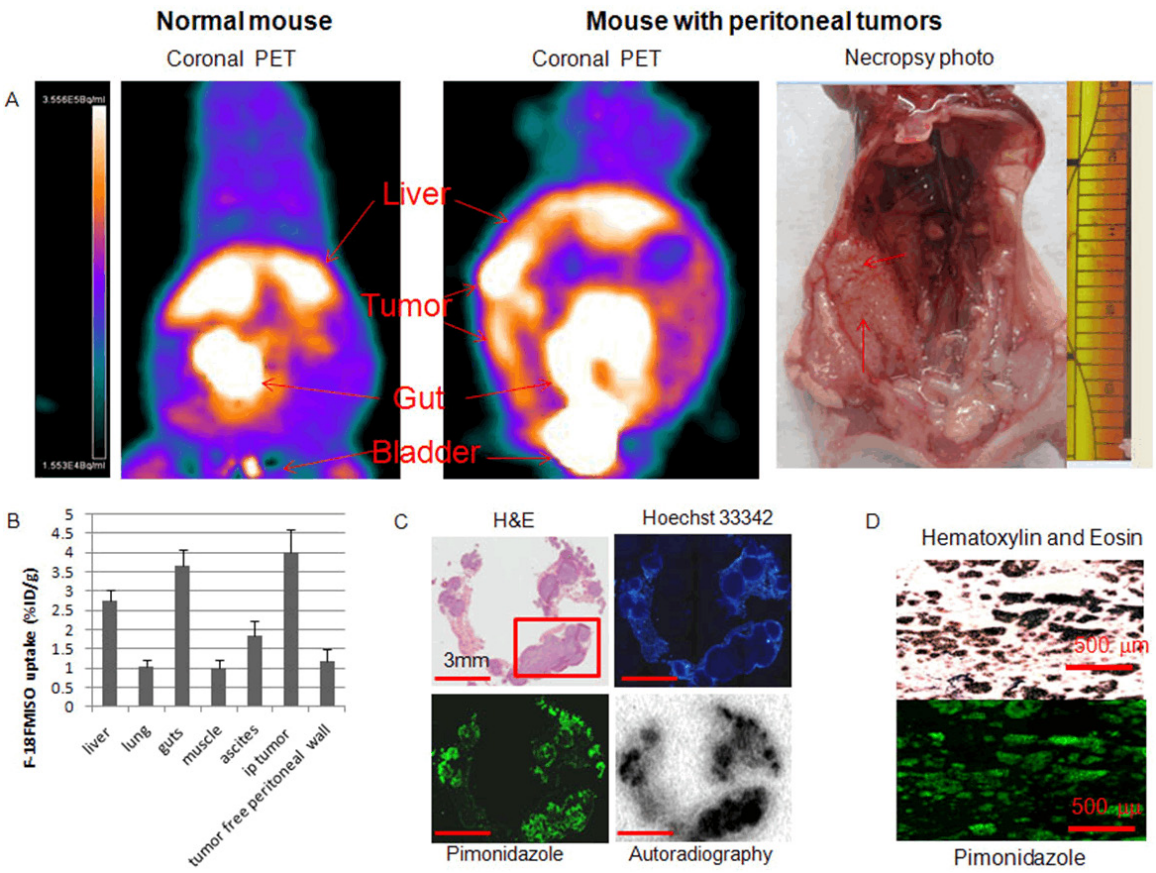

Figure 1. A. PET coronal slices of intraperitoneal distribution of ^{18}F-misonidazole in a peritoneal disease–free mouse (left) and a mouse with peritoneal metastases after A549 cells inoculation (middle) with necropsy- confirmed peritoneal wall carcinomas (right). High radioactivity accumulation was found on the abdominal wall as indicated and the overall background in the peritoneal cavity (excluding guts) was apparently higher than control. B. ^{18}F-misonidazole (^{18}F-FMISO) distribution in A549 i.p. tumors in mice (n=5). C. Multiple individual lesions attaching to the peritoneal wall where PET imaging had revealed a high level of ^{18}F-misonidazole: Hematoxylin and Eosin stain showing multiple individual micrometastases (generally less 1mm in diameter) which had little Hoechst 33342 uptake, associated with a high fraction of pimonidazole binding and high ^{18}F-misonidazole accumulation by autoradiography. D. Single cells or ascites tumors harvested from ascites of the mouse were stained-positive for pimonidazole, Hematoxylin and Eosin stain provides as a reference. All scale bars are as indicated.

tumors before freezing and embedding in O.C.T. Ascites tumors were harvested, washed with cold PBS to remove red blood cells, frozen and embedded in O.C.T.. For all tumor samples, 5 contiguous 7-μm- thick tissue sections were cut using a 3050S cryostat microtome (Leica, Inc) and adhered to poly-L-lysine-coated glass microscope slides (Fisher Scientific, Inc).

^{18}F-misonidazole digital autoradiography

Digital autoradiography was obtained by placing the tumor sections in a film cassette against an imaging plate as described previously [9, 10, 27]. The same plate was used through the experiments; the plate was exposed for 20h and read by a Cyclone Plus imaging system (PerkinElmer, Inc). The images were analyzed by OptiQuant software (PerkinElmer Inc.) and compared with pimonidazole, bromodeoxyuridine and Hoechst 33342 immunohistochemical staining.

Pimonidazole, glucose transporter-1 and bromodeoxyuridine immunohistochemical staining

Pimonidazole, bromodeoxyuridine and Hoechst 33342 images were obtained after autoradiography [7, 9, 10, 27]. In order to minimize issues associated with section alignment and registration, the same tumor section used for autoradiography or contiguous adjacent sections were used for all images. Briefly, slides were air-dried, fixed in cold acetone (4°C) for 20 min, and incubated with SuperBlock (37515, Pierce

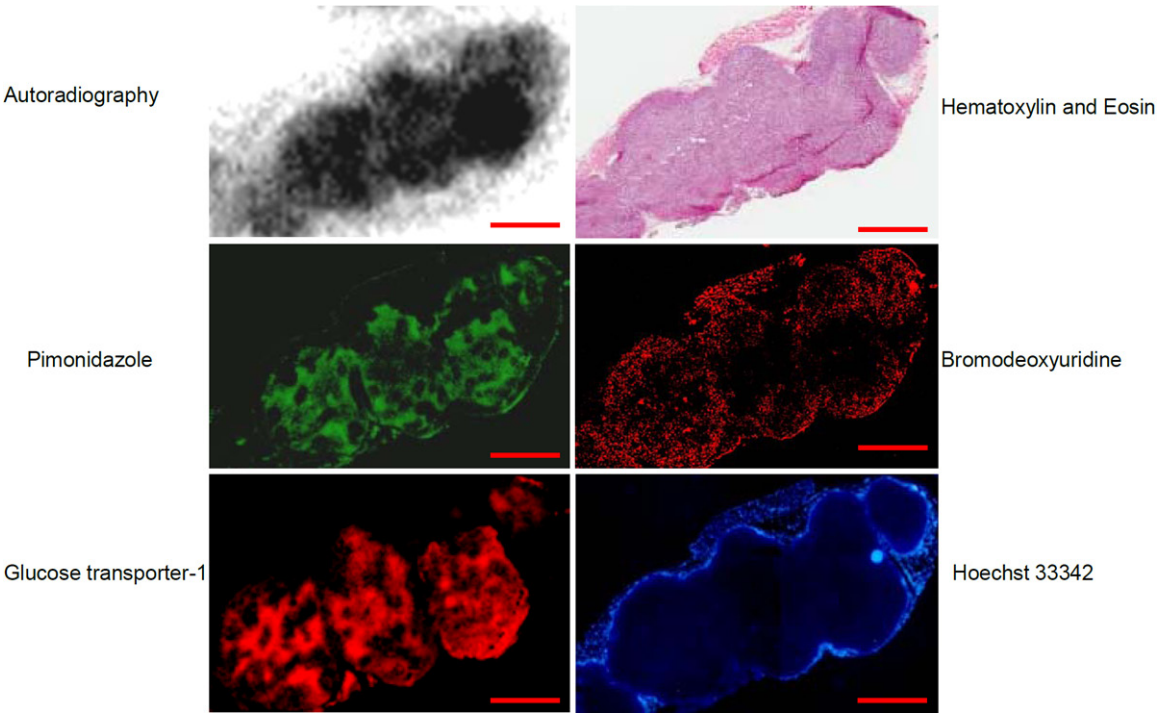

Figure 2. The relationship between ^{18}F-misonidazole uptake and hypoxia, proliferation and perfusion in A549 peritoneal micrometastases. High levels of ^{18}F-misonidazole uptake, pimonidazole binding and glucose transporter-1 expression are co-localized with each other and with low proliferation (by bromodeoxyuridine) and perfusion (Hoechst 33342). All scale bars are 1mm.

Biotechnology, Rockford, IL) at room temperature for 30 min. All antibodies were also applied in SuperBlock. Sections were then incubated with FITC conjugated anti-pimonidazole monoclonal antibody (Hypoxyprobe Inc, Burlington, MA), diluted 1:25, for 1h at room temperature. Glucose transporter-1 staining was performed on the same section as that stained for pimonidazole by incubating for 1 h at room temperature with rabbit anti- glucose transporter-1 polyclonal antibody (Millipore) diluted 1:50. Sections were washed 3 times in PBS, each wash lasting 5 min, and incubated for 1 h at room temperature with either AlexaFluor568-conjugated goat anti-rabbit antibody (1:100, Molecular Probes) and washed again. For bromodeoxyuridine staining, adjacent sections to those used for pimonidazole were treated with 2N HCl for 10 min at room temperature followed by 0.1M Borax for 10 min at room temperature. Sections were then exposed to AlexaFluor594-conjugated anti-bromodeoxyuridine antibody (1:20 dilution, Molecular Probes, Eugene, OR) for 1h at room temperature.

Immunohistochemical staining images were acquired at ×40 magnification using a Nikon Eclipse E800 fluorescence microscope (Nikon America Inc., Melville, NY) equipped with a motorized stage (Ludi Electronic Products Ltd., Hawthorne, NY). Hoechst 33342 and pimonidazole were imaged using blue and green filters, respectively. Bromodeoxyuridine was imaged using a red filter. H&E was imaged by light microscopy. Microscopic images were coregistered using Photoshop 7.0 (Adobe, San Jose, CA).

Results

We evaluated the intraperitoneal tumor activity accumulation of ^{18}F-misonidazole in peritoneal disease–free mice (n=3) and mice with A549 and HTB177 peritoneal metastases (5 mice for each cell line). All image sets for each animal were visually examined using a rotating (cine) three-dimensional display. **Figure 1A** shows representative PET coronal slices: In metastases-bearing mice, high radioactivity accumulation was found on the left side of abdominal wall and the overall background in the peritoneal cavity (excluding the intestines) was apparently higher than in the normal mouse. Necropsy revealed that the left peritoneal wall

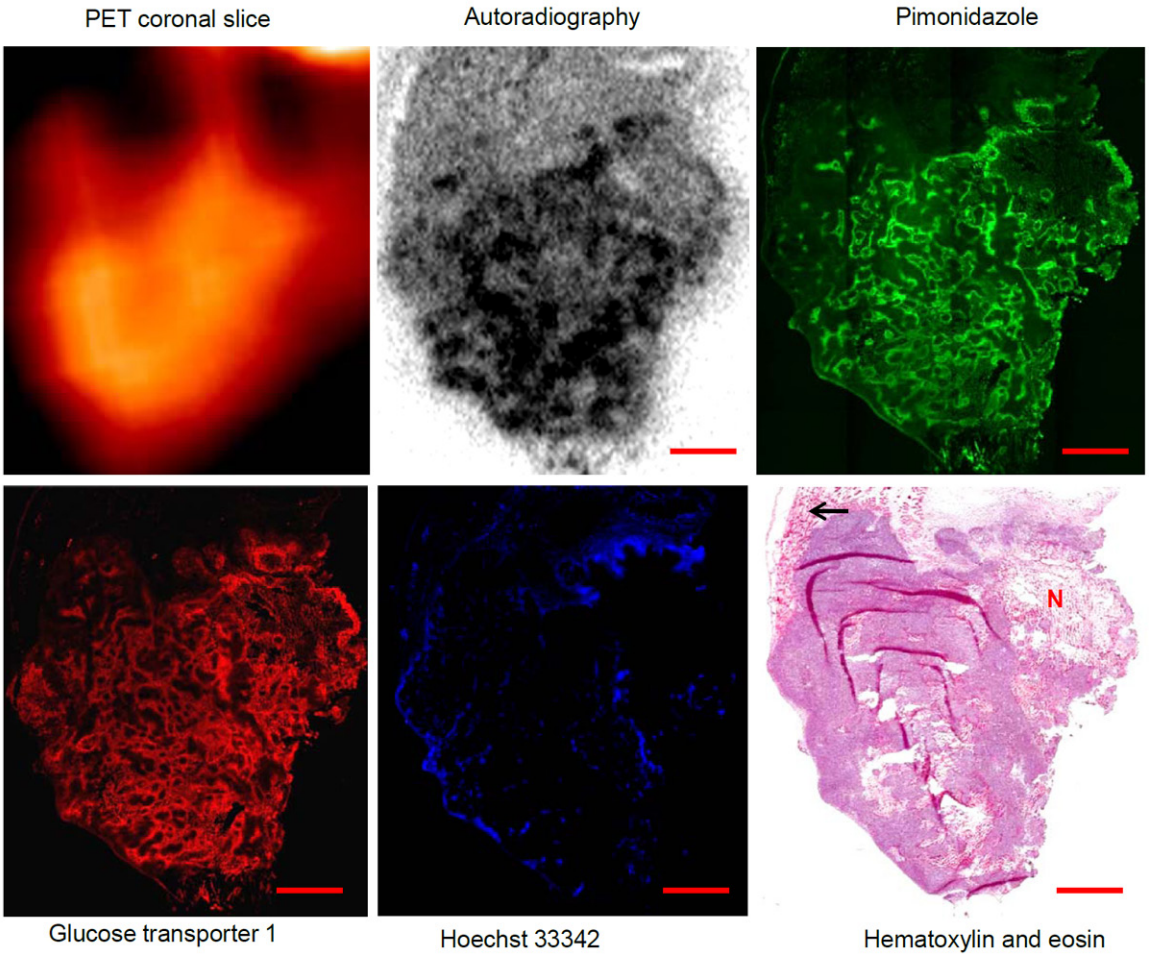

Figure 3. Intratumoral distribution of ^{18}F-misonidazole in a macroscopic HTB177 subcutaneous xenograft by PET and autoradiography and its relationship to tumor microenvironment. Autoradiography, pimonidazole, glucose transporter-1 expression, and Hoechst 33342 images were obtained from the same frozen tissue section, Hematoxylin and Eosin stain from an adjacent section. Necrosis (N) and stroma (as arrow indicated) are associated with low ^{18}F activity. All scale bars are 2 mm.

was the site of multiple individual tiny lesions. In both the disease-free and metastases-bearing mice, there was significant uptake of ^{18}F-misonidazole in the gut and bladder and to a lesser extent in the liver (**Figure 1B**). Tumors from the left peritoneal wall were removed for sectioning (**Figure 1C**), H & E staining demonstrated multiple individual micrometastases (generally less 1mm in diameter), some of them fused together. The micrometastases had little Hoechst 33342 uptake indicating a lack of blood perfusion, and a high fraction of pimonidazole binding and high ^{18}F-misonidazole accumulation, indicating severely hypoxic tissue. There was little ^{18}F-misonidazole accumulation in the stroma. Approximately 3.5 ml of ascites fluid was collected from the peritoneal cavity, and single cells or ascites tumors (~300 μl) were harvested by centrifugation and these stained positive for pimonidazole (**Figure 1D**). Therefore, ^{18}F-misonidazole PET is able to detect micrometastases in the peritoneal cavity. Similar results were observed in HTB177 peritoneal metastases, although in this cell line model ascites did not develop frequently.

Figure 2 shows the relationship between ^{18}F-misonidazole uptake and hypoxia, proliferation and perfusion in A549 peritoneal micrometastases collection (as shown in region of interest of **Figure 1C**). There was spatial co-localization between ^{18}F-misonidazole uptake pimonidazole binding and glucose transporter-1 expression. Such regions also

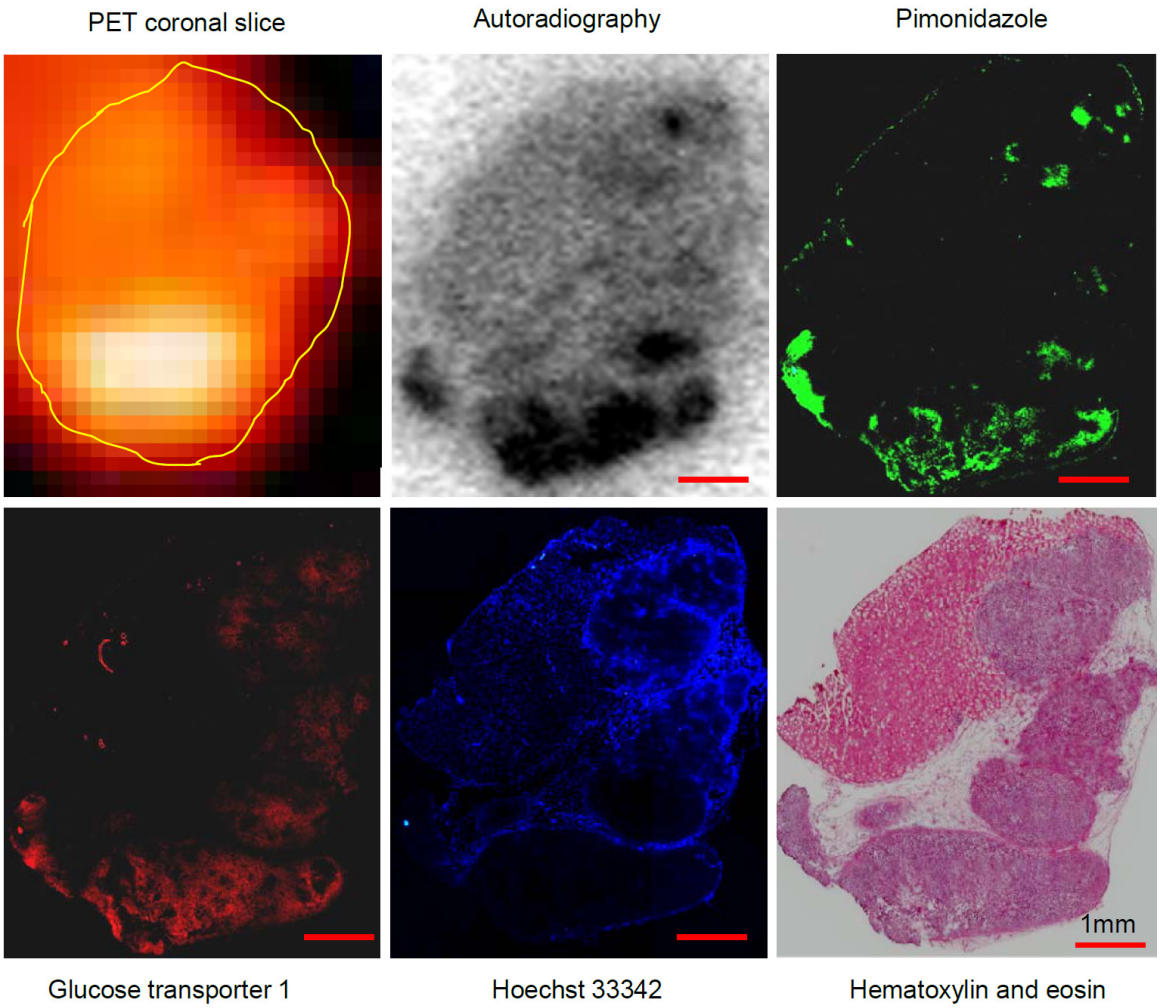

Figure 4. Intratumoral distribution of ^{18}F-misonidazole in a macroscopic A549 subcutaneous xenograft by PET and autoradiography and its relationship to tumor microenvironment. Autoradiography, pimonidazole, glucose transporter-1 expression, Hoechst 33342 and Hematoxylin and Eosin stains were obtained from the same frozen tissue section. Stroma and pimonidzole -negative cancer cells associated with low ^{18}F-misonidazole accumulation. Glucose transporter-1 expressing regions are much wider than those positive for pimonidazole. All scale bars are 1 mm.

displayed low perfusion and proliferation (by Hoechst 33342 and bromodeoxyuridine, respectively). Conversely, the peripheral rim of the lesions had low ^{18}F-misonidazole and pimonidazole accumulation, but stained positive for bromodeoxyuridine, suggesting that the tissue was well oxygenated and contained dividing cells.

Figure 3 shows a representative ^{18}F-misonidazole PET mid-coronal slice of a macroscopic HTB177 subcutaneous tumor, showing considerable heterogeneity in the spatial distribution of the tracer. Autoradiography, pimonidazole, glucose transporter-1 expression, and Hoechst 33342 images were obtained on the same section and H and E staining was performed on an adjacent section. ^{18}F-misonidazole co-localized with pimonidazole, which was roughly similar to glucose transporter 1, and these regions mutually excluded Hoechst 33342. Regions of low pimonidazole binding (such as in the upper left corner) also had low ^{18}F-misonidazole uptake. Necrosis and stroma were also associated with low ^{18}F-misonidazole activity. Therefore, ^{18}F-misonidazole accumulated in hypoxic cancer cells, and low radioactivity regions were either nonhypoxic cancer tissue or stroma and necrosis. In this study, co-registration between PET slices and frozen section autoradiography

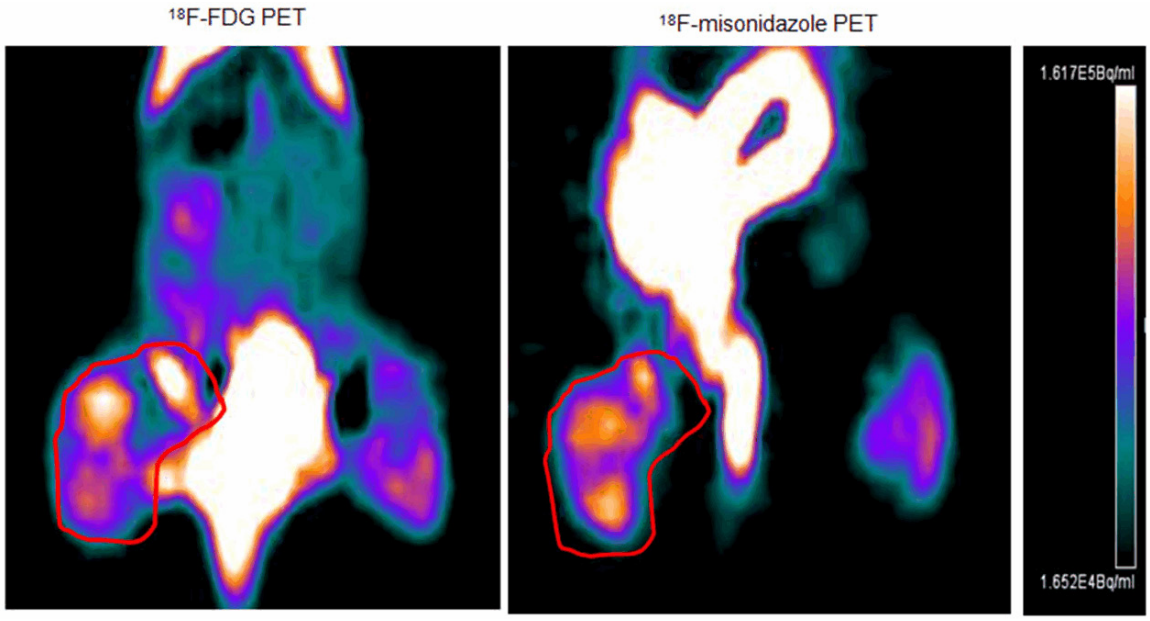

Figure 5. Comparing intratumoral distribution of ^{18}F-FDG and ^{18}F-misonidazole by PET in the same tumor. Intratumoral distribution of ^{18}F-FDG and ^{18}F-misonidazole were roughly similar, though mismatched regions were apparent. Images were obtained 24 h apart; animals were fast overnight for ^{18}F-FDG study.

was not attempted. Of note, although glucose transporter-1 expression was roughly similar to pimonidazole binding, the former appeared to be much wider than the latter. Subcutaneous A549 xenografts yielded similar results. **Figure 4** shows a representative ^{18}F-misonidazole PET A549 mid-coronal slice, with autoradiography, pimonidazole, glucose-transporter-1 Hoechst 33342, and H and E staining performed as before. Again, ^{18}F-misonidazole accumulated only in poorly perfused viable tumor tissue. We have previously reported that the intratumoral distribution of ^{18}F-FDG and ^{18}F-misonidazole detected by autoradiography was similar and that both tracers accumulated in hypoxic zones [27]. Here we extended our observation of ^{18}F-FDG and ^{18}F-misonidazole using PET on the same tumor bearing animals. ^{18}F-FDG and ^{18}F-misonidazole PET scans were performed separated by a 24 h interval in the same animals (4 mice). A set of representative images is presented in **Figure 5**. The intratumoral distribution of ^{18}F-FDG and ^{18}F-misonidazole were roughly similar, although areas of mismatch were apparent. In another study, serial ^{18}F-FDG and ^{18}F-misonidazole PET imaging indicated that neither ^{18}F-FDG nor ^{18}F-misonidazole intratumoral distribution PET imaging could be reproduced on the second scan, possibly because of dynamic changes in hypoxia during the 24 h interval [28].

Discussion

We have previously reported the existence of severe hypoxia in microscopic tumors derived from HT29 and HCT-8 colorectal cancer cells grown intraperitoneally in nude mice [7-10]. In the current study, we extended our evaluation of the hypoxic status in microscopic tumors to non-small cell lung cancer cell lines and included the use of the radiolabeled hypoxia tracer, ^{18}F-misonidazole, as a means of verification. Importantly we have confirmed that ^{18}F-misonidazole is able to detect hypoxic cancer cells in microscopic peritoneal metastases and macroscopic xenografts; the hypoxia specific binding feature of ^{18}F-misonidazole was subsequently verified by autoradiography and immunohistochemical examinations of exogenous and endogenous hypoxia markers of frozen sections obtained after PET scans of the same animals.

HT29 and HCT-8 microscopic tumors of submillimeter dimensions growing in peritoneal cavities were severely hypoxic as judged by high levels of pimonidazole binding and carbonic anhydrase IX expression, and indirectly by the absence of blood perfusion [7]. Accordingly, we hypothesized that severe hypoxia would be a general feature of micrometastases regardless of cancer type and anatomic location [8].

To test this hypothesis, in the current study, we introduced non-small cell lung cancer cells to the peritoneal cavity to generate peritoneal carcinomatosis. Our data indicated that microscopic tumors with sub-millimeter diameters were severely hypoxic and lack functional blood perfusion (**Figures 1** and **2**). In addition, proliferative cells were only located on the periphery in these microscopic tumors, while the cores were hypoxic and non-proliferative. The data supports our hypothesis that microscopic tumors are severely hypoxic. The effect of anatomic locations, in addition to peritoneal cavity, on hypoxia status of micrometastases is still under investigation in liver, brain and other organs.

Presence of severe hypoxia of peritoneal micrometastases may cause in anticancer therapy resistance; hypoxic cells are more resistant than aerobic cells to ionizing radiation and chemotherapy. On the other hand, the presence of severe hypoxia may have its advantage as a specific target for molecular imaging of micrometastatic disease, which may be difficult to detect with current anatomic imaging modalities like CT and/or MRI. In the present study we have examined the capacity of ^{18}F-misonidazole PET for this purpose, and found that the collection of multiple micrometastases was able to be detected noninvasively by ^{18}F-misonidazole PET (**Figure 1**). Furthermore, there was an apparent increase in ^{18}F-misonidazole activity in ascites (**Figure 1**); in which approximately 300 μl of single cancer cells and clusters of cancer cells were harvested from 3.5 ml of ascites, all were stained positive for pimonidazole (**Figure 1C**). We have found previously that ascites tumors of HT29 were severely hypoxic as well and direct measurement by oxyLite O_2 probe indicated that *p*O2 of ascites was less 1 mmHg in the model [29]. Therefore, abnormal accumulation of ^{18}F-misonidazole in the peritoneal cavity would be a sign of the presence of micrometastases and increased radioactivity in ascites may be a sign of presence of cancer cells which are hypoxic. Current PET technique may be impractical for directly assessing hypoxia in individual microscopic tumors which are too small to be seen on images [8], but we have confirmed here that a collection of multiple micrometastases can be detected.

In the current study, we used correlative imaging methodologies to examine the uptake of ^{18}F-misonidazole in both microscopic and macroscopic tumors and relate this to hypoxia, perfusion and proliferation. ^{18}F-misonidazole uptake, visualized by digital autoradiography, was compared with immunofluorescent visualization of pimonidazole binding and glucose-transporter-1 expression. We found that ^{18}F-misonidazole uptake closely associated with -pimonidazole binding, while well oxygenated cancer cells (negative for pimonidazole), as well as regions of stroma and necrosis had low ^{18}F-misonidazole accumulation (**Figures 1-4**), confirming our previous report with this model [27]. ^{18}F-misonidazole in PET may noninvasively detect hypoxic status in non-small cell lung cancer cells either at microscopic or macroscopic level. Since the presence of hypoxia is a general feature of solid malignancies [3-6], to some extent, ^{18}F-misonidazole PET would be useful to distinguished cancers from benign diseases, such as in patients with lung nodules; this issue may need further investigation.

We have recently reported that in non-small cell lung cancer mouse models ^{18}F-FDG also mostly accumulates in hypoxic and non-proliferative cancer cells, and thus behaves similarly to ^{18}F-misonidazole in terms of its intratumoral distribution [27]. Tumor microenvironment is fluctuating, and changes in hypoxia have been reported in experimental xenografts growing in animals [30] and solid cancers in patients [24], even in a time scale of 1-3 days. In this study, we have compared ^{18}F-misonidazole and ^{18}F-FDG in the same tumors by PET scans performed 24 h apart. **Figure 5** shows that while the intratumoral distribution of ^{18}F-FDG and ^{18}F-misonidazole were roughly similar, some mismatch was present, possibly due to changes in hypoxia occurring over 24 h. Interestingly, our preliminary data of serial ^{18}F-FDG and ^{18}F-misonidazole PET studies indicated that for neither tracer could the intratumoral distribution on day 1 be fully replicated on day 2 [28].

As shown in **Figure 3** and **Figure 4**, ^{18}F-misonidazole accumulated in hypoxic regions of xenografts, and therefore can be used to assess the hypoxic volume of the tumor. We found that low ^{18}F-misonidazole radioactivity regions were either nonhypoxic cancer cells or noncancerous stroma and necrosis. Although hypoxia plays an important role in cancer biology, the presence of oxic cancer cells cannot be ignored. Oxic cancer cells

are highly proliferative, and therefore, are of importance for cancer management. ^{18}F-fluorothymidine generally accumulates in proliferating cancer cells [27]; therefore, if ^{18}F-fluorothymidine is injected immediately after ^{18}F-misonidazole PET, the combined scans should visualize both hypoxic and oxic (proliferative) cancer cells: in a future study, we will evaluate this proposal. We have recently found that the combination of ^{18}F-FDG and ^{18}F-fluorothymidine with a single PET can visualize more viable cancer cells than either individual tracer (unpublished data). ^{18}F-FDG shares a similar intratumoral distribution pattern with ^{18}F-misonidazole [27], so that a combination of ^{18}F-FDG and^{18}F-misonidazole for a single PET scan may not provide additional information than either of them alone.

Conclusion

Microscopic peritoneal metastases of human non-small cell lung cancer growing in mice are severely hypoxic. ^{18}F-misonidazole PET is feasible to noninvasively image hypoxia not only in macroscopic tumors but also in the micrometastases. Accordingly, ^{18}F-misonidazole PET is promising for micrometastatic diseases detection.

Acknowledgments

We thank James Russell, PhD, at Memorial Sloan-Kettering Cancer Center (New York NY) for editing the article. This study was supported by Kentucky Lung Cancer Research Program Award, partially by National Natural Science Foundation of China (81130028) and Science and Technique Foundation of Heilongjiang Province (GA12C302). The authors have no conflict of interest relevant to this article.

Address correspondence to: Dr. Xiao-Feng Li, Department of Diagnostic Radiology, University of Louisville School of Medicine, 530 S. Jackson Street, CCB-C07, Louisville KY, 40202 USA. Phone: 502-217-8285; Fax: 502-852-1754; E-mail: linucmed@gmail.com; xiao-feng.li@louisville.edu or Dr. Baozhong Shen, Department of Radiology, the 4th Hospital of Harbin Medical University, 37 Yinhang Street, Harbin 150001, China. E-mail: shenbzh@vip.sina.com

References

[1] Howlader N, Noone AM, Krapcho M, Neyman N, Aminou R, Waldron W, et al (eds). SEER Cancer Statistics Review, 1975-2008, National Cancer Institute. Bethesda, MD, *http://seer.cancer.gov/csr/1975_2008/*, posted to the SEER web site, 2011.

[2] Soon YY, Stockler MR, Askie LM, Boyer MJ. Duration of Chemotherapy for Advanced Non-Small-Cell Lung Cancer: A Systematic Review and Meta-Analysis of Randomized Trials. J Clin Oncol 2009; 27: 3277-83.

[3] Thomlinson R, Gray L. The histological structure of some human lung cancers and the possible implications for radiotherapy. Br J Cancer 1955; 9: 539-49.

[4] Höckel M, Schlenger K, Knoop C, Vaupel P. Oxygenation of carcinomas of the uterine cervix: evaluation by computerized O_2 tension measurements. Cancer Res 1991; 51: 6098-102.

[5] Höckel M, Knoop C, Schlenger K, Vorndran B, Knapstein PG, Vaupel P. Intratumoral pO2 histography as predictive assay in advanced cancer of the uterine cervix. Adv Exp Med Biol 1994; 345: 445-50.

[6] Koch CJ and Evans SM. Non-invasive PET and SPECT imaging of tissue hypoxia using isotopically labeled 2-nitroimidazoles. In: Wilson DF, Evans SM, Biaglow J, Pastuszko A, editors. Oxygen transport to tissue. Adv Exp Med Biol 2003; 510: 285-292.

[7] Li XF, Carlin S, Urano M, Russell J, Ling CC, O'Donoghue JA. Visualization of hypoxia in microscopic tumors by immunofluorescent microscopy. Cancer Res 2007; 67: 7646-53.

[8] Li XF and O'Donoghue JA. Hypoxia in microscopic tumors. Cancer Letters 2008; 264: 172-80.

[9] Li XF, Sun X, Ma Y, Suehiro M, Zhang M, Russell J, Humm JL, Ling CC, O'Donoghue JA. Detection of hypoxia in microscopic tumors using 131I-labeled iodo-azomycin galactopyranoside (131I-IAZGP) digital autoradiography. Eur J Nucl Med Mol Imaging 2010; 37: 339–48.

[10] Li XF, Ma Y, Sun X, Humm JL, Ling CC, O'Donoghue JA. High 18F-fluorodeoxyglucose (18F-FDG) uptake in microscopic peritoneal tumors requires physiological hypoxia. J Nucl Med 2010; 51: 632-8.

[11] Brizel DM, Scully SP, Harrelson JM, Layfield LJ, Bean JM, Prosnitz LR, Dewhirst MW. Tumor oxygenation predicts for the likelihood of distant metastases in human soft tissue sarcoma. Cancer Res 1996; 56: 941-3.

[12] Brizel DM, Hage WD, Dodge RK, Munley MT, Piantadosi CA, Dewhirst MW. Hyperbaric oxygen improves tumor radiation response significantly more than carbogen/nicotinamide. Radiat Res 1997; 147: 715-20.

[13] Ljungkvist AS, Bussink J, Kaanders JH, van der Kogel AJ. Dynamics of tumor hypoxia mea-

sured with bioreductive hypoxic cell markers. Radiat Res 2007; 167: 127-45.

[14] Bentzen L, Keiding S, Horsman MR, Falborg L, Hansen SB, Overgaard J. Feasibility of detecting hypoxia in experimental mouse tumours with 18F-fluorinated tracers and positron emission tomography--a study evaluating [18F] Fluoro-2-deoxy-D-glucose. Acta Oncol 2000; 39: 629-637.

[15] Alauddin MM. Positron emission tomography (PET) imaging with (18)F-based radiotracers. Am J Nucl Med Mol Imaging 2012; 2: 55-76.

[16] Troost EG, Laverman P, Philippens ME, Lok J, van der Kogel AJ, Oyen WJ, Boerman OC, Kaanders JH, Bussink J. Correlation of [18F] FMISO autoradiography and pimonidazole immunohistochemistry in human head and neck carcinoma xenografts. Eur J Nucl Med Mol Imaging 2008; 35: 1803-11.

[17] Vavere AL, Lewis JS. Cu-ATSM: a radiopharmaceutical for the PET imaging of hypoxia. Dalton Trans 2007; 4893-902.

[18] Tatum JL, Kelloff GJ, Gillies RJ, Arbeit JM, Brown JM, Chao KS, Chapman JD, Eckelman WC, Fyles AW, Giaccia AJ, Hill RP, Koch CJ, Krishna MC, Krohn KA, Lewis JS, Mason RP, Melillo G, Padhani AR, Powis G, Rajendran JG, Reba R, Robinson SP, Semenza GL, Swartz HM, Vaupel P, Yang D, Croft B, Hoffman J, Liu G, Stone H, Sullivan D. Hypoxia: importance in tumor biology, noninvasive measurement by imaging, and value of its measurement in the management of cancer therapy. Int J Radiat Biol 2006; 82: 699-757.

[19] O'Donoghue JA, Zanzonico P, Pugachev A, Wen B, Smith-Jones P, Cai S, Burnazi E, Finn RD, Burgman P, Ruan S, Lewis JS, Welch MJ, Ling CC, Humm JL. Assessment of regional tumor hypoxia using 18F-fluoromisonidazole and 64Cu(II)-diacetyl-bis(N4-methylthiosemicarbazone) positron emission tomography: Comparative study featuring microPET imaging, Po2 probe measurement, autoradiography, and fluorescent microscopy in the R3327-AT and FaDu rat tumor models. Int J Radiat Oncol Biol Phys 2005; 61: 1493-502.

[20] Iyer RV, Engelhardt EL, Stobbe CC, Schneider RF, Chapman JD. Preclinical assessment of hypoxic marker specificity and sensitivity. Int J Radiat Oncol Biol Phys 1998; 42: 741-745.

[21] Zanzonico P, O'Donoghue J, Chapman JD, Schneider R, Cai S, Larson S, Wen B, Chen Y, Finn R, Ruan S, Gerweck L, Humm J, Ling C. Iodine-124-labeled iodo-azomycin-galactoside imaging of tumor hypoxia in mice with serial microPET scanning. Eur J Nucl Med Mol Imaging 2004; 31: 117-28.

[22] Riedl CC, Brader P, Zanzonico PB, Chun YS, Woo Y, Singh P, Carlin S, Wen B, Ling CC, Hricak H, Fong Y. Imaging hypoxia in orthotopic rat liver tumors with iodine 124-labeled iodoazomycin galactopyranoside PET. Radiology 2008; 248: 561-570.

[23] Vera P, Bohn P, Edet-Sanson A, Salles A, Hapdey S, Gardin I, Ménard JF, Modzelewski R, Thiberville L, Dubray B. Simultaneous positron emission tomography (PET) assessment of metabolism with ^{18}F-fluoro-2-deoxy-d-glucose (FDG), proliferation with ^{18}F-fluoro-thymidine (FLT), and hypoxia with^{18}fluoro-misonidazole (F-miso) before and during radiotherapy in patients with non-small-cell lung cancer (NSCLC): a pilot study. Radiother Oncol 2011; 98: 109-16.

[24] Nehmeh SA, Lee NY, Schröder H, Squire O, Zanzonico PB, Erdi YE, Greco C, Mageras G, Pham HS, Larson SM, Ling CC, Humm JL. Reproducibility of intratumor distribution of (18) F-fluoromisonidazole in head and neck cancer. Int J Radiat Oncol Biol Phys 2008; 70: 235-42.

[25] Yasuda K, Onimaru R, Okamoto S, Shiga T, Katoh N, Tsuchiya K, Suzuki R, Takeuchi W, Kuge Y, Tamaki N, Shirato H. (18)F]fluoromisonidazole and a new PET system with semiconductor detectors and a depth of interaction system for intensity modulated radiation therapy for nasopharyngeal cancer. Int J Radiat Oncol Biol Phys 2013; 85: 142-7.

[26] Mammar H, Kerrou K, Nataf V, Pontvert D, Clemenceau S, Lot G, George B, Polivka M, Mokhtari K, Ferrand R, Feuvret L, Habrand JL, Pouysségur J, Mazure N, Talbot JN. Positron Emission Tomography/Computed Tomography Imaging of Residual Skull Base Chordoma Before Radiotherapy Using Fluoromisonidazole and Fluorodeoxyglucose: Potential Consequences for Dose Painting. Int J Radiat Oncol Biol Phys 2012; 84: 681-7.

[27] Huang T, Civelek AC, Li J, Jiang H, Ng CK, Postel GC, Shen B, Li XF. Tumor microenvironment–dependent ^{18}F-FDG, ^{18}F-Fluorothymidine, and ^{18}F-misonidazole uptake: a pilot study in mouse models of human non–small cell lung cancer. J Nucl Med 2012; 53: 1262-8.

[28] Li XF, Huang T, Jiang H, Li J, Zheng H, Ng C. Molecular imaging of spatial and temporal heterogeneity of tumor micro-environment in mouse models of non-small cell lung cancer macroscopic xenografts and micro-metastases [abstract]. In: Proceedings of the 103rd Annual Meeting of the American Association for Cancer Research; 2012 Mar 31-Apr 4; Chicago, IL. Philadelphia (PA): AACR; Cancer Res 2012; 72 Suppl 8: Abstract nr 2439. doi: 1538-7445. AM2012-2439.

[29] Li XF, Civelek AC. Severe hypoxia of ascites and increased ^{18}F-FDG uptake in ascites carcino-

mas: a paradox to Warburg effect. J Nucl Med 2012; 53 suppl: 222.
[30] Ljungkvist AS, Bussink J, Kaanders JH, Rijken PF, Begg AC, Raleigh JA, van der Kogel AJ. Hypoxic cell turnover in different solid tumor lines. Int J Radiat Oncol Biol Phys 2005; 62: 1157-68.